

Polydispersity and assembling phenomena of native and reactive dye-labelled nanocellulose

Selestina Gorgieva · Robert Vogrinčič ·
Vanja Kokol

Received: 8 June 2015 / Accepted: 9 September 2015 / Published online: 23 September 2015
© Springer Science+Business Media Dordrecht 2015

Abstract The assembling (self-association vs. aggregation or agglomeration) of highly polydispersed nanocelluloses (NCs) is a well-known but difficult to identify phenomena. In this research complementary analytical tools were applied for tracking and assessing this phenomena under different conditions (base vs. buffer) using both native and dye-labelled cellulose nanofibrils (CNFs) and cellulose nanocrystals. For this purpose, dichlorotriazine-type reactive blue 4 (RB4) dye was covalently (through alkyl-aryl ether bond) and regioselectively (to C6–OH groups) attached to the NC, being identified by ATR-FTIR and ^{13}C CP/MAS solid-state NMR spectroscopies, and quantified by UV–Vis spectroscopy. The introduced RB4's anthraquinone (i.e. hydrophobic) moieties evoked aggregation of those CNFs being quantified from the shifting and broadening of size-distribution profiles within differential light scattering analysis and their ζ -potential reduction. In addition, their high polydispersity profiles was assessed by qualitatively supported differential centrifugal sedimentation, nanoparticle

tracking analysis, and transmission electron microscopy. A desorption of chemically non-bonded, yet highly substantive (i.e. partially or fully hydrolysed), dye from both types of NCs was also identified by capillary electrophoresis, which simultaneously excluded the non-labelled fractions, thus obtaining free dye-absent NC dispersions. Finally, labelling extent-triggered separation within the RB4-labelled CNFs was identified by applying the micellar capillary electrophoresis, thus confirming the conformational changes affecting NCs' hydrodynamic (size) profiles.

Keywords Nanocellulose · Reactive dye · Labelling · Polydispersity · Aggregation · Conformation

Introduction

Semi-crystalline nanofibrils (CNFs) and highly-crystalline cellulose nanocrystals (CNCs) have been growing in importance over the last decade due to their lightness, large surface areas, extraordinarily strong modules (Jiang and Hsieh 2013), low thermal expansion coefficients (Dufresne 2013) as well as biocompatibility (Lin and Dufresne 2014; Jorfi and Foster 2014), and biodegradability. As such, nanocellulose (NC) has become a promising nano-material in differently engineered forms and compositions, such as nanocomposites/hybrids, nano-additives, nano-

S. Gorgieva · R. Vogrinčič · V. Kokol (✉)
Institute for Engineering Materials and Design, University
of Maribor, Smetanova ul 17, 2000 Maribor, Slovenia
e-mail: vanja.kokol@um.si

S. Gorgieva
e-mail: selestina.gorgieva@um.si

sensors and nano-filters for various technical (Lindström and Aulin 2014) and (bio)medical (Lin and Dufresne 2014) applications.

The NCs' usage generally relies on the abundant hydroxyl groups and their susceptibilities for chemical modifications (i.e. esterification, etherification, oxidation, silylation, polymer grafting, hydrophobisation, etc. (Eyley and Thielemans 2014; Missoum et al. 2013)), which in turn may alter their macroscopic behaviour, such as speeding-up the already existing (via inter-molecular H-bonds) self-association versus agglomeration tendencies (Zoppe 2011). In some technical areas, as e.g. paper sheets' development, the self-association of NC is thus a desirable phenomenon (Ioelovich 2009), whilst in others, as e.g. composite production, the aggregation may seriously diminish the reinforcing properties (Kim et al. 2009), and as such need to be controlled or ultimately avoided. The NC application in biomedicine (e.g. optical bio-imaging, biosensor, and photodynamic therapy) is limited by similar issues, where high and unavoidable heterogeneity (size, shape and surface related) and assembling phenomena on the one hand as well as high swelling ability and thus gelling phenomena on the other (Choi and Frangioni 2010) hinder their verification and validation. In fact, the *in vivo* behaviour of the NC [the mechanism of internalisation, diffusion and trafficking within the cells, as with their fates inside the cells as accumulation and/or elimination (Domingues et al. 2014)] is generally believed to be dependent on the physico-chemical relationships at their nano-bio interfaces (Lin and Dufresne 2014). The toxicities of CNCs have thus recently been shown (Roman 2015) to depend strongly on CNC charge and degree of aggregation, which determines their final shapes and dimensions. However, following the EU regulation initiative (REG EU), it is necessary to consider the safety issues and risk assessment aspects, being affected not only by the purity of NC itself (being related to its production process) but mainly by its nano-declaration profile (being related to the sizes of its mono, aggregate or agglomerate structures).

Apart from the processing issues, the characterisation of NC's heterogenicities and self-assembling phenomena is another limitation. The celluloses' intrinsic lack of fluorescence limits the number of available techniques and methods for NC tracking and localisation, and consequently their optical data

storage, being of utmost importance in biochemical, bio analytical, medical and other areas of their utilisations. Their visualisations by scanning electron microscopy (SEM) or atomic force microscopy (AFM) require time and effort for detailed observation due to small observation fields (AFM in particular) making these techniques prohibitive for detailed analysis (Iwamoto et al. 2013). As an alternative, fluorescent labelling (using FITC (Dong and Roman 2007), isothiocyanate, succinimidyl ester, pyrene, dichlorotriazine (Abitbol et al. 2013; Huang et al. 2013), etc. allows extensive microscopy studies (from trivial, distribution patterns' observations up to distribution and cellular uptake follow-up (Generalova et al. 2009). However, the macro-scale effect from nanoscale modification of a NC surface is very often neglected, which again leads to artefacts during the characterisation processes.

In this respect, the presented study examines the feasibilities of different analytical tools (DLS, DCS, NTA, and TEM) for identifying and evaluating polydispersity, in the same way as assembling the phenomena of native versus dye-labelled NC. For that purpose, CNFs and CNCs were separately labelled with hydrophobic dichlorotriazine-type reactive dye (RB4) and evaluated for labelling efficiencies by means of coupling mechanism using ATR-FTIR and ^{13}C CP/MAS solid-state NMR spectroscopies, coupling efficacy by CE/MKCE and quantity by UV-Vis spectroscopy.

Experimental

Materials

The cellulose nanofibrils (CNFs) were prepared from cellulose sludge according to the procedure reported by Jonoobi et al. (2012). The cellulose sludge was first suspended within distilled water and dispersed in water to a concentration of 3 wt% by using a mechanical blender (Silverson L4RT, England) at 3000 rpm for 10 min. Then, the suspension was passed through an ultra-fine grinder (MKCA 6-3, Masuko, Japan) for 30 min at 1440 rpm thus forming gel-like suspension. The produced CNFs were chain-like structures within diameters of the 10–70 nm range and the length of micrometer scale, bearing 73 ± 1.2 mmol/kg of

carboxylic groups (as confirmed by potentiometric titration with a twin-burette instrument Mettler Toledo T70).

The cellulose nanocrystals (CNC) were extracted from the cellulose bioethanol residue, by following a modified version of the procedure described by (Oksman et al. 2011). Lignin and the extractives were removed after de-waxing, bleaching and cleaning. The purified cellulose was made into 2 wt% suspensions, mixed by shear mixture and passed through the homogeniser ten times in order to obtain a thick gel of CNC. The polyethylene glycol was added in traces in order to allow concentration-obtained diluted dispersions. The produced CNC showed a typical cellulose mono-crystalline structure with a measured diameter of 5–10 nm, bearing of about 150 ± 5.1 mmol/kg of carboxylic groups as well as traces of sulphate groups introduced by sulphuric acid treatment (Liu et al. 2013).

The dichlorotriazine dye reactive blue 4 (RB4) with Mw of 637.43 g/mol, sodium tetraborate ($\text{Na}_2\text{B}_4\text{O}_7$), sodium dodecyl sulphate (SDS), dimethyl sulfoxide (DMSO), sodium carbonate (Na_2CO_3), sodium chloride (NaCl), and sucrose ($\text{C}_{12}\text{H}_{22}\text{O}_{11}$) were supplied from Sigma Aldrich and used without further purification.

NC labelling

The RB4 labelling of NC was performed according to the procedure recommended by the dye manufacturer (pattern card by ICI Colours and Fine Chemicals) for cellulose dyeing. For that purpose, 10 mL of 0.5 % w/v NC water dispersions were sonicated for 2 min at 25 % amplitude using the Ultrasonic Processor (SONICS Vibra cellTM VCX 750, Sonics & Materials, Inc., USA). Afterwards, different amounts of dye were added to final concentrations of 0.5, 2 or 4 % w/v, and mixtures were shaken at 130 min^{-1} and 30 °C for 10 min, followed by triple-steps addition of 0.35 g NaCl (0.025, 0.075 and 0.25 g) at 10 min intervals during continuous shaking. This was followed by two-steps addition of 0.04 g Na_2CO_3 (0.002 and 0.018 g) at 5 min intervals, and kept for an additional 45 min to complete the reaction. The samples were multiply washed-out, first with EtOH and afterwards with deionised water to remove the unreactive dye (being spectrophotometrically followed in parallel), and further stored at 4 °C until further examinations. The

reference samples were prepared, following the same procedure as described above, without addition of the dye.

NC characterisation

ATR-FTIR spectroscopy analysis

The spectra's of the native and RB4-labelled NC were recorded using a Perkin-Elmer Spectrum One FTIR spectrometer with a Golden Gate ATR attachment and a diamond crystal. The absorbance measurements were carried out within the range of $650\text{--}4000 \text{ cm}^{-1}$, with 16 scans and a resolution of 4 cm^{-1} , and the spectrum 5.0.2 software program was applied for data analysis. All the measurements were carried out in duplicate.

¹³C CP/MAS solid-state NMR spectroscopy analysis

¹³C CP/MAS solid-state NMR spectroscopy analyses of the native and RB4-labelled NC samples were carried out using a solid-state NMR spectrometer (Agilent Technologies NMR System 600 MHz) by using its 3.2 mm NB double resonance HX MAS probe. The NC powder samples were placed within a zirconia sample tube. The ¹³C CP/MAS conditions were as follows: resonance frequency 150.83 MHz, spinning rate 16 kHz, number of points 2048, and number of scans 1000 at 25 °C. Hexa-methyl-benzene ($\text{C}_{12}\text{H}_{18}$; δ 17.3 ppm) was used as a standard for ¹³C. The crystallinity index (CI) was determined according to Park et al. (2009) by separating the C4 region of the spectrum into crystalline and amorphous peaks, and calculated by dividing the area of the crystalline peak (86–93 ppm) by the total area assigned to the C4 peak (80–93 ppm).

The overlapped peaks within both ATR-FTIR and ¹³C CP/MAS spectral lines were resolved by the deconvolution/curve-fitting procedure using PeakFit v4.12 program software.

UV-Vis spectrophotometrical analysis

The dye consumption during the labelling process was spectrophotometrically followed at 598 nm by analysing the RB4-containing dyeing baths as well as respective washing solutions using a Tecan UV-Vis micro plate reader. A prepared calibration curve was

used for estimation of the dye amount per NC dry mass (mmol/g), being calculated as the difference between concentrations of dye in a solution prior and during labelling, also including the concentrations of dye in the washing baths, normalised to sample mass in grams (g).

Dynamic light scattering (DLS) analysis

The ζ -potential and size analysis of native and RB4-labelled NC dispersions were carried out on a Zetasizer (Nano ZS ZEN360, Malvern instrument LTD., UK) at 20 ± 0.1 °C using the cell ZEN1010, applying the following parameters: a material refractive index of 1.47, dispersion refractive index of 1.33, and viscosity of 0.8872 cP. A field of 40 V was applied across the nominal electrode spacing of 16 mm. The samples were prepared at concentrations of 0.005 % w/v in Milli-Q water and measured over a pH range from 2 to 10, being adjusted using 0.1 M NaOH and 0.1 M HCl, respectively. In parallel, dispersions were prepared in the same concentrations using 20 mM borate buffer, with or without the addition of 50 mM SDS and pH adjustment to pH 9.3 by using 0.1 M NaOH. The average values, as well as the standard deviation of the mean values, were calculated from at least four individual measurements.

Differential centrifugal sedimentation (DCS) analysis

The size and distribution of native and RB4-labelled NC dispersions (0.5 % w/v) were evaluated in Milli-Q water by the CPS disc centrifuge (DC 24000, CPS Instruments Inc.) at 20 ± 0.1 °C. The 8–24 % w/v of sucrose solution in Milli-Q water was used and filled over nine steps into the disc, starting with the dilution of the highest density and finishing with 0.5 mL of dodecane, for diminishing the evaporation process. A disc rotation speed of 15,000 rpm was used to set up the analysis. The calibration was performed by injecting 10 μ L of 0.377 μ m sized PVC particles as calibration standard (Analytik Ltd.) before measuring each sample. The same volume of 1 % w/v prevortexed NC/water dispersions was injected into the disc centrifuge. The repeatability of CPS measurements was examined over three runs for each sample and data averaging was applied by the system software CPSV 95.

Nanoparticle tracking analysis (NTA)

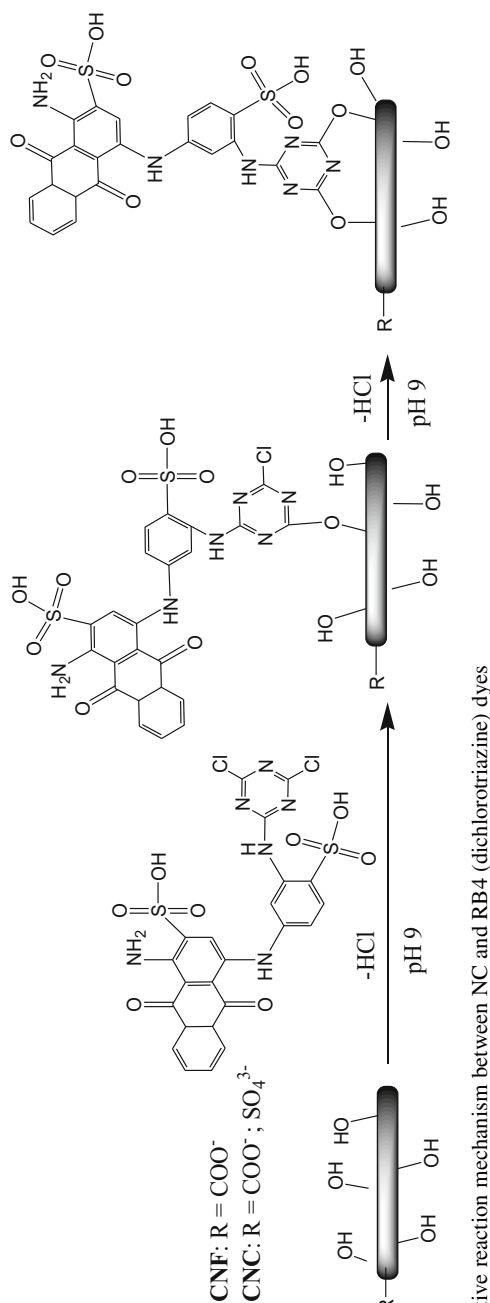
The NTA measurements of native and RB4-labelled NC dispersions of 0.01 % w/v concentration were performed at 20 ± 0.1 °C using a NanoSight LM10 instrument with finely focused (red) laser beams of 635 nm. The suspended NC, being subsequently injected below a quartz prism on the laser beam path, scattered the light in a manner easily visualised with 20 \times magnification microscopic objective, fitted to a conventional optical microscope onto which was mounted a highly sensitivity camera (operating at 30 frames per second). The camera subsequently captures a video file of particles moving under Brownian motion within a field of approximately 100 μ m \times 80 μ m \times 10 μ m. For each sample at least three runs were applied by keeping the instrument set-up parameters constant in order to ensure measurement accuracy.

Transmission electron microscopy (TEM) analysis

TECNAI G2 20 TEM microscopy was used for visualisation of size and potential conformation changes of NCs as a consequence of the RB4-labelling procedure. A 10 μ L of native and RB4-labelled NC dispersions of 0.001 % w/v concentration were deposited on the carbon coated-copper grids (Formvar, Agar Sci.) for that purpose and allowed to dry overnight. Analyses were carried out with an accelerating voltage of 120 kV and sample-dependent exposure time with up to 60,000 \times magnification.

Capillary electrophoresis (CE) and micellar CE (MKCE) analysis

The CE/MKCE analyses of native and RB4-labelled NCs were performed using diode array detector (DAD) equipped to the Agilent CE3D G-1600 capillary electrophoresis system. The extended (bubble factor 3) light path was provided by using 56 cm long fused silica capillary with 75 μ m internal diameter. Prior to analysis, the capillary was rinsed for 20 min with 1 M NaOH, followed by additional 10 min washing with Milli-Q water and final 20 min washing with 20 mM sodium borate buffer (pH 9.3) used as a background electrolyte (BGE). The MKCE analyses were performed in the presence of 50 mM SDS being added in BGE. Before each run the capillary was



Scheme 1 Tentative reaction mechanism between NC and RB4 (dichlorotriazine) dyes

preconditioned with 1 M NaOH for 2 min, Milli Q water for 1 min and BGE for an additional 2 min. The 3 mM thiourea was added to the BGE as an internal marker. Furthermore, NC dispersions of 0.0005 % w/v concentration were intensively mixed and injected hydrodynamically at 50 mbar for 50 s, followed by a plug of BGE at 50 mbar for 4 s. The 25 kV voltage (producing the 150 μ A electrical charges) and constant (25 \pm 0.1 $^{\circ}$ C) temperature were applied as input parameters. The DAD detection was performed at 200 \pm 5 and 598 \pm 4 nm, respectively, according to the absorption maximums of polysaccharides (Shi and Fu 2011) and RB4 dye, respectively.

Results and discussion

Qualitative and quantitative evaluation of NC labelling

The reactive dye (RB4) used for NC labelling contains the triazinyl ring with two highly reactive chloride atoms capable of nucleophilic substitution with deprotonated cellulose hydroxyl groups under alkaline conditions (Srikulkit and Pornsuriyasak 1998), according to the simplified, tentative mechanism being presented in Scheme 1.

The mechanism of covalent coupling of RB4 to the NC, being related to the new alkyl-aryl type ether group formed, was confirmed by ATR-FTIR spectral analysis (Fig. 1) demonstrating typical cellulose-related vibrations for both types of NC (Xu et al. 2013). The vibration regions of new ether moiety, presented by C–O–C asymmetrical (1000–1300 cm^{-1}) and symmetrical stretching (1070–1150 cm^{-1}) highly overlapped with celluloses' glycosidic bonds, being visible in native CNFs and CNCs at about 1055 and 1035 cm^{-1} , respectively. However, a closer look over this region (red selected area) reveals diverse profiles for both NCs after labelling when compared to their native forms, same as the evolution of a new band in the C–O–C region at 1100 cm^{-1} which is evidenced by the ether formation. This is additionally supported by a shifting of the RB4-related aromatic ring (C=C) vibration at \sim 1411 (Christiane et al. 2013) to \sim 1428 cm^{-1} in the labelled CNFs and CNCs, respectively, same as the sulphonate group's asymmetrical and symmetrical stretching vibrations from

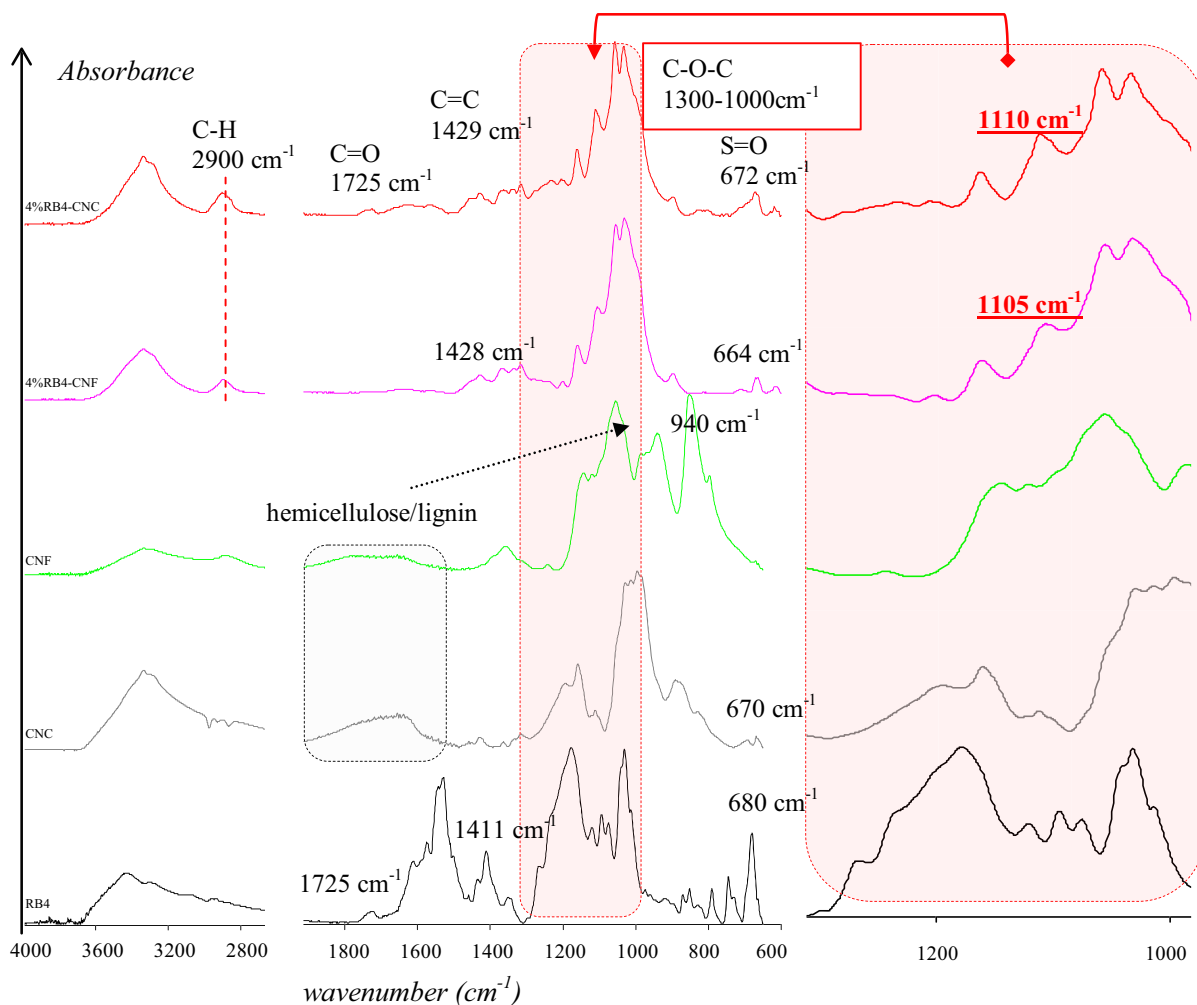


Fig. 1 ATR-FTIR spectra of native and RB4-labelled CNFs and CNCs

~ 680 to ~ 660 cm^{-1} (CNFs) and ~ 670 cm^{-1} (CNCs), both indicating bonding effect.

On the other hand, the O–H stretching region (3000 – 3600 cm^{-1}) revealed the splitting of the mono-distributed, broad vibration line in CNFs after RB4 labelling, which together with the evolution of C–H related vibration (~ 2900 cm^{-1}) may be a consequence of introduced hydrophobicity by dye-related anthraquinone moiety. Besides, the peaks at about 730 – 790 cm^{-1} (within RB4) spectra, being related to C–Cl vibrations (Christiane et al. 2013), disappearing after the labelling reactions, indicating Cl ions substitution with cellulose OH groups, according to the well-known reaction mechanism.

In addition, the broad adsorption within the 1700 – 1800 cm^{-1} region in native NC (especially in CNCs due to the presence of aldehyde/carboxylic groups), as well as intensive vibration at 940 cm^{-1} (in CNFs) may indicate on the lignin and hemicellulose residues (Mariño et al. 2015; Rosa et al. 2010) being absent after RB4 labelling, probably due to their extraction under alkaline conditions (Sun 2009).

The ^{13}C CP/MAS NMR analysis of native and RB4-labelled NC provides additional information on the mechanism and the regioselectivity of the RB4 labelling reaction. The noticeable signals within the 50 – 110 ppm chemical shifts region (Fig. 2, above) are seen, being attributable to different carbons' cellulose

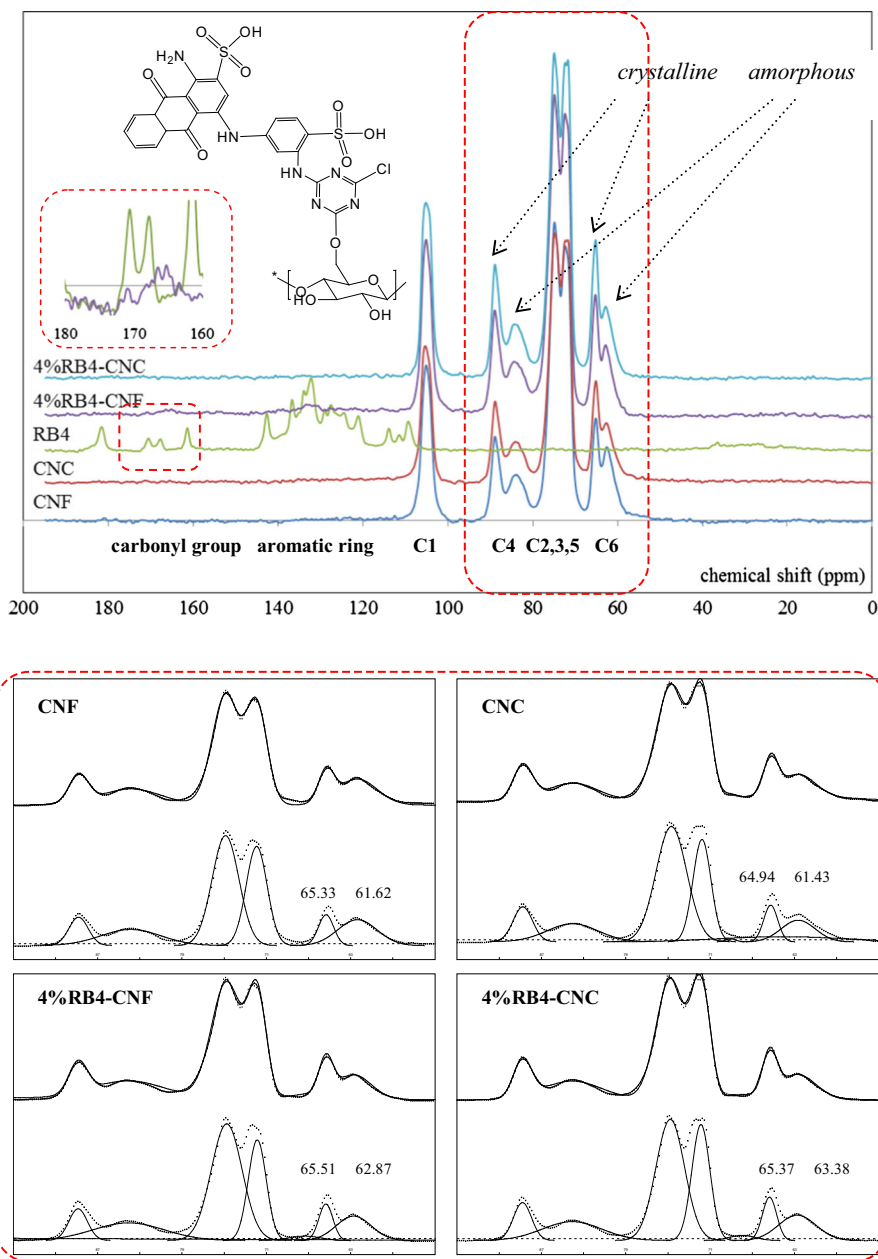


Fig. 2 Solid state ^{13}C CP/MAS NMR spectra of native and RB4-labelled CNFs and CNCs (*above*) with de-convoluted 55–95 ppm region (*below*)

carbons: the region at 58–68 ppm assigned to C6 (containing crystalline and amorphous parts), the cluster of signals at 68–80 ppm assigned to C2, C3 and C5, the region at 80–91 ppm assigned to C4 (containing crystalline and amorphous parts), and finally the region at 101–109 ppm which can be assigned to C1 (Halonen et al. 2012).

Due to the well-known up-field shift effects in the resonances of the adjacent carbons within glucopyranosic compounds during their modification via hydroxyl groups (Granja et al. 2001), the de-convoluted spectral lines were compared within the 55–95 ppm region (Fig. 2, below). In the case of the C6 position shifts at about 1.2/2 ppm within

amorphous and 0.2/0.4 ppm in crystalline regions were observed after RB4-labelling of CNFs and CNCs, respectively. This confirms that the modifications generally occur at the C6 positions of accessible amorphous domains (CNCs) or amorphous regions (CNFs). On the other hand, small and inconsistent changes within the C2, C3 and C5 regions of both NC

types, coupled with small (<0.1 ppm) shifting of C4 towards higher resonance, indicate modifications the adjacent C3 position. Indeed, C4 carbon is involved in glycosidic linkage and hence unavailable for substitution and its small shifting can be attributed to the steric, gamma effect following the cellulose modification.

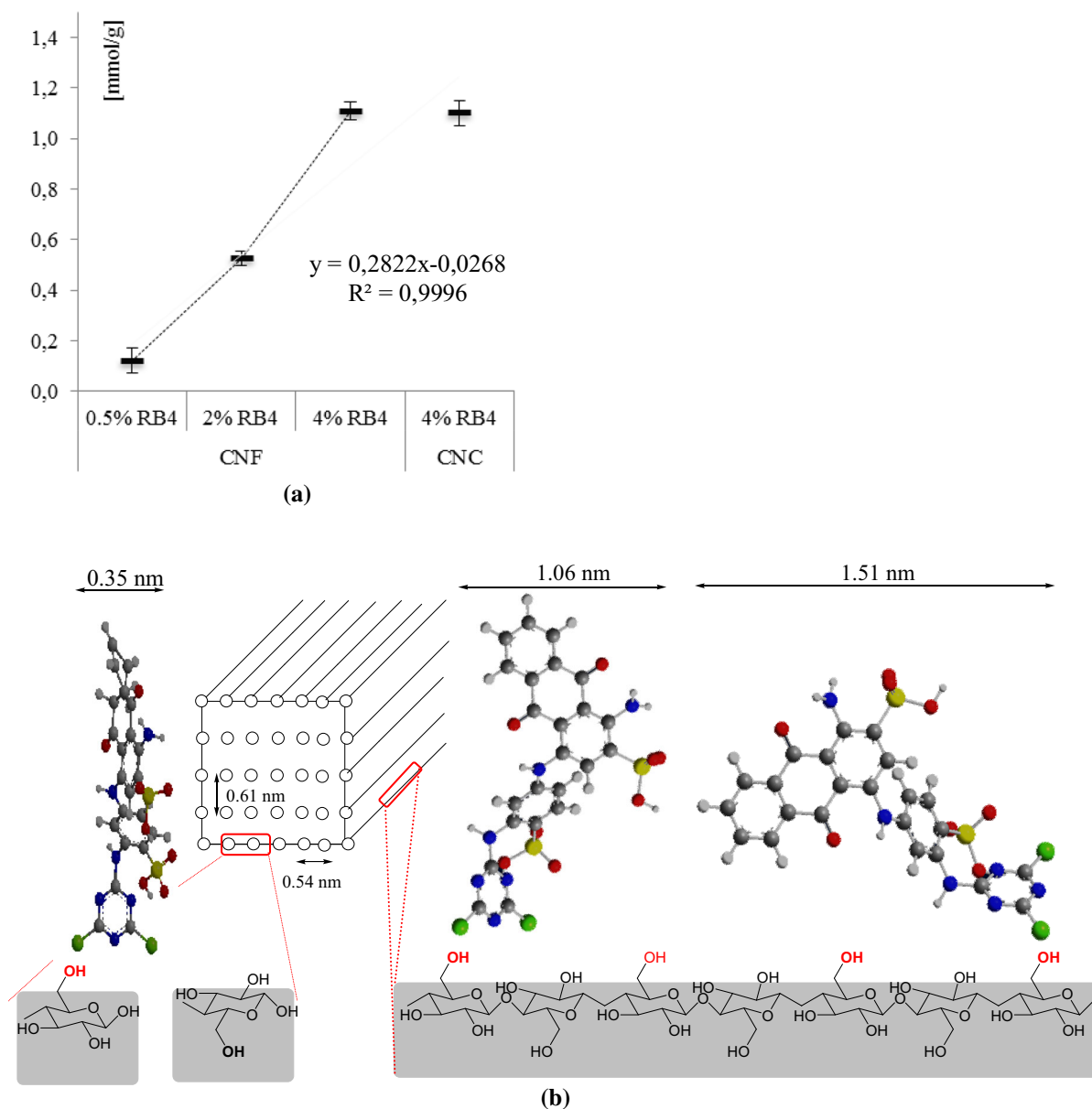


Fig. 3 **a** The RB4-labelling efficiencies of CNFs and CNCs quantified by UV–Vis spectrophotometry with respective linear fitting equations relating to the starting dye concentrations and dye exhausted by each type of NC (mmol/g). **b** Schematic

anticipation of RB4 molecules upwards/laid-down orientations in line (*right*) or perpendicular (*left*) to the NC surface by considering NCs' containing cellulose type I crystals

In addition, a small yet noticeable (included figure in Fig. 2, above) RB4-related signal at 130 ppm, same as C=O related (split) signal at 167/170 ppm, being for 2 ppm left-shifted within 4 % RB4-CNFs (165/166 ppm), supports the FTIR findings by confirming RB4 presence and binding, respectively.

The labelling efficacy was followed spectrophotometrically by evaluations of the dyeing baths and the washing solutions (Fig. 3a), which indirectly measures the amount of remaining dye attached to the NC. Based on the calculated data, the same reaction yield ($1.1 + 0.035$ mmol/g) was obtained for both NC types in the presence of equal RB4 concentrations (4 % w/v), even if it was expected that higher OH accessibility within the amorphous regions of the CNFs, combined with larger OH derivatisation during the CNCs' processing towards carboxylic (~ 150 vs. 73 mmol/kg in CNFs), as well as the presence of sulphate ester groups, would provide superior values for CNFs.

However, as this analytical tool does not distinguish between adsorbed and chemically-bonded dye, the theoretical calculations [being simplified due to well-known difficulties when obtaining the exact number of NC-surface exposed OH (Dufresne 2012)], were performed in accordance to a recent review (Eyley and Thielemans 2014).

By comparing the roughly estimated values of surface accessible hydroxyls onto NC, being within the range of 2–3 mmol/g (Dufresne 2012), this calculation fits well for one-layer attachment and consequently covalent bonding of RB4 due to the higher affinity of C1 towards cellulose OH groups rather than water. The reported value count was only half of the accessible hydroxyl groups of cellulose (red selected OH/C6/within the scheme of Fig. 3b) which were available for reaction, whereas the other half were buried within the crystalline particle as a consequence of the twofold screw axis of the cellulose chain (Habibi et al. 2010). When considering the RB4 dimensions (Sun et al. 2013) within the same cellulose chain (Fig. 3b, right), the dye molecule covered a surface of about 1.06 nm in its upward orientation towards NC or ~ 4 OH groups, whilst in laid-down orientation a surface of $1.509 \text{ nm} \times 0.35 \text{ nm}$ or ~ 6 OH groups. In the perpendicular direction to the cellulose chain (Fig. 3b, left) RB4 molecule covered ~ 3 OH groups of cellulose, being calculated by 0.54–0.61 nm distance between cellulose chains

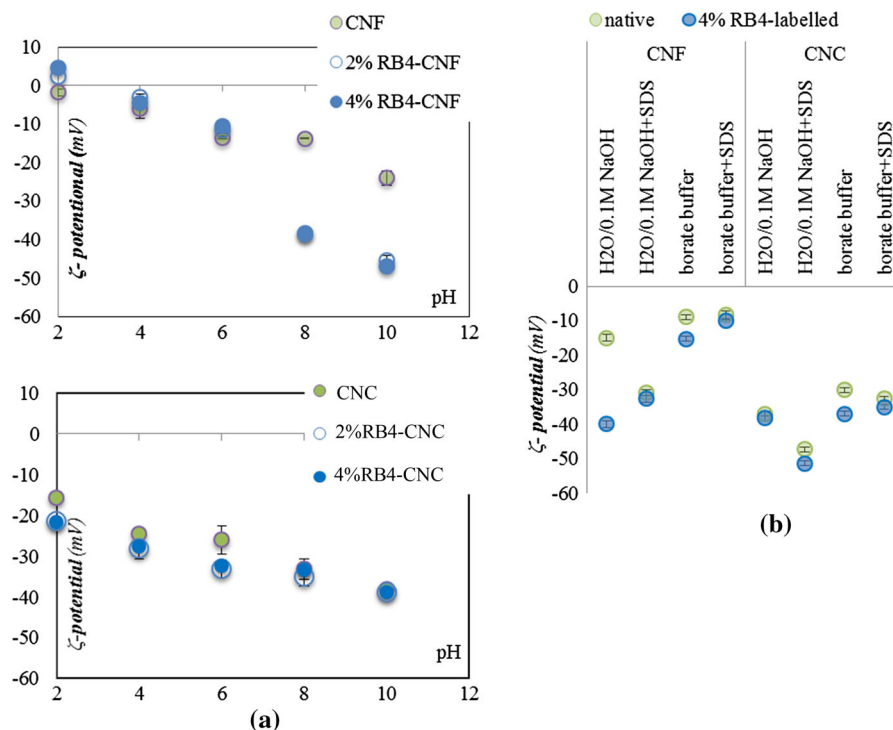
within a single cellulose I type crystal (Bendahou et al. 2014). Therefore, maximum 1 mmol/g of RB4 (1/3 of 3 mmol/g) was sterically accommodated during its upward-perpendicular orientation, being almost identical to our calculation. This assumption is valid for CNCs already possessing modified OH groups, implying the potential presence of adsorbed dye. This was further examined by CE/MKCE means and is presented in one of the following paragraphs. Oppositely, the more-amorphous CNFs that under dyeing conditions (high pH) become even more accessible due to swelling phenomena prohibit such assumptions and at the same time imply higher bonding efficacy.

Characterisations of native and labelled-NC by DLS analysis

The ζ -potential and size measurements were performed for indicating the labelling effect on NC self-assembling. As presented in Fig. 4a, both types of NC show negative ζ -potential at pH >2, being reduced to ~ -20 and -40 mV at pH 10 in CNFs and CNCs, respectively, due to the deprotonations of the presence of carboxylic (in both NC) and sulphate (in CNC) groups (being identified also by FTIR). The RB4 dye contained two sulphonate groups, the primary and secondary amino groups, same as heteroatoms (the nitrogens) within the benzene ring, all of which contribute to the whole net charge of labelled-NC, according to their pKa values. In that respect a sharp reduction in CNFs' ζ -potential value after RB4-labelling was observed in the pH 6–8 region, being close to the RB4 pKa [at pH 5.2 (Sun et al. 2013)]. In addition an increase was identified below the transition pH due to the dye protonation, bringing a change of ~ 50 mV from the pH 10 to pH 2 with insignificant difference between both (2 and 4 %) RB4 used concentration. On the other hand, for ~ 10 mV lower ζ -potential values were measured in the cases of RB4-labelled CNCs by using the same dye concentrations, which in accordance with spectrophotometrical quantification may indicate different dye orientation.

In accordance with the CE/MKCE analysis being obtained in a borate buffer of pH 9.3 without/with SDS addition, the ζ -potential profile of NC and RB4-labelled NC was estimated under the same conditions. The results (Fig. 4b) demonstrate the labelling-related but RB4-concentration-independent reduction of ζ -

Fig. 4 The ζ -potential analyses of native and RB4-labelled CNFs and CNCs **a** within the 2–10 pH range, and **b** at pH 9.3 being adjusted with 0.1 M NaOH or by using a 20 mM borate buffer, without and with the addition of 50 mM SDS



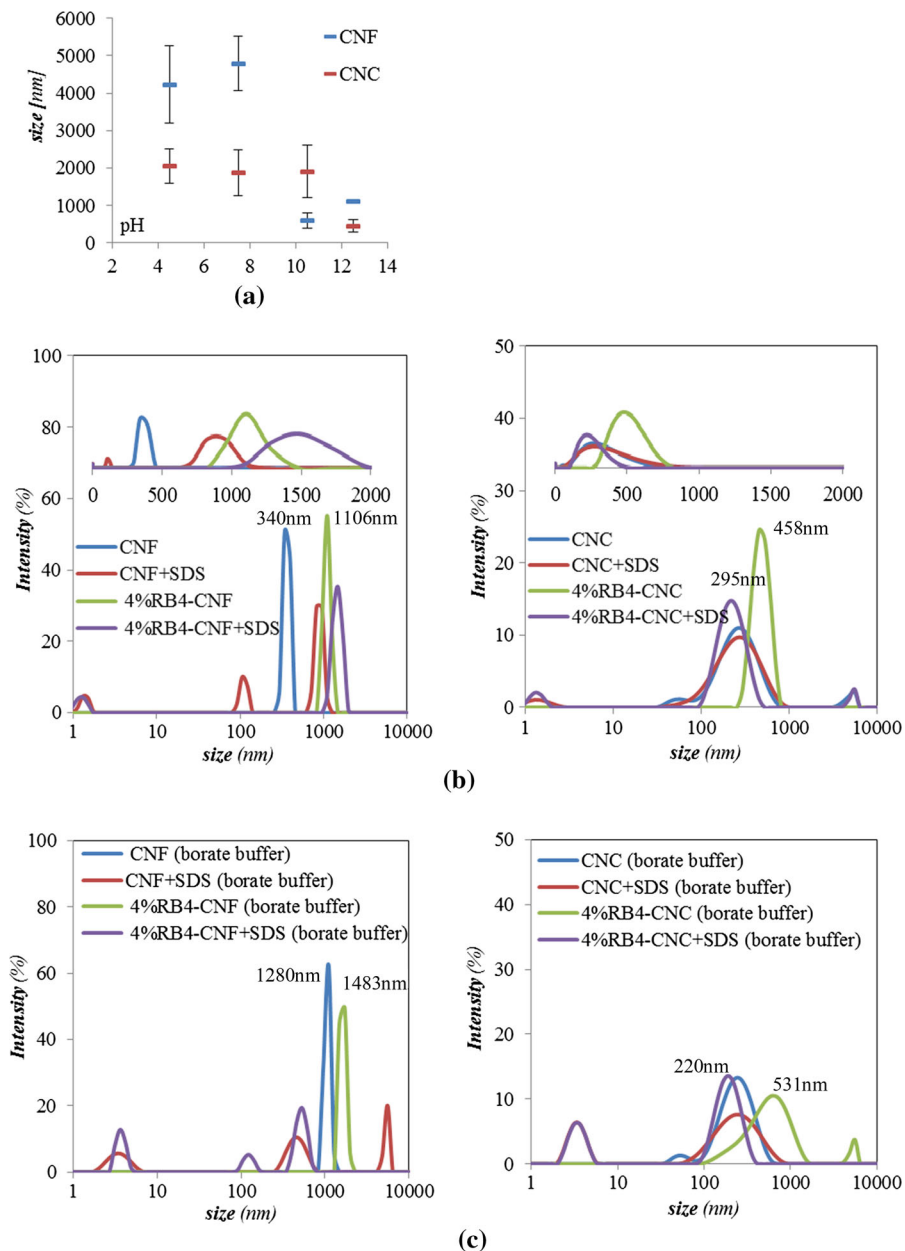
potential, which (as will be shown later) negatively affect the labelled-NC dispersion stability, leading to aggregation (and size increase). In fact, the nano-scale structures with highly-specific surfaces have increased thermodynamic potential, causing the instabilities of nano objects and, according to the thermodynamics rule (to achieve a more stable state) tend to decrease their specific surfaces (Islam et al. 2013); this phenomena is even magnified by nanoscale dimensions decrease (Fall 2013). Besides, the presence of a borate buffer (instead of water) additionally decreases the NC ζ -potential, same as the presence of anionic SDS (to water or borate buffer), which at the same time reduces the differences within NC before and after the labelling to insignificant values. Such a behaviour can be a consequence of CNFs' charges being shielded by attracted SDS molecules, the sulphate groups of which being upwardly oriented, irrespective of partially hydrophobic RB4-labelled CNFs. Very similar ζ -potential variations in the functions of the measuring media were identified for respective CNC samples. Indeed, equalisation of charge between RB4-labelled and non-labelled NCs in borate buffer or borate buffer in the presence of SDS media is valuable for CE/MKCE analysis, due to

overcoming the charge-related differences during the separation process, thus focusing on changes being functions of size only.

The DLS sizes analyses were performed as comparisons rather than for quantification purposes due to the spherical particle limitations of this technique. Moreover, the fact that the intensity of the measured scattered light is proportional to the sixth power of the particle diameter makes this technique very sensitive to the presence of large particles, and as such suitable for the identification of aggregate processes within NC.

The first observation was directed towards the pH-dependent average sizes of native NCs (Fig. 5a) and the relatively large standard deviations being related to their intrinsic heterogeneous natures as with electrostatic interactions (arising from the carboxylic vs. sulphate surface groups) and related entanglements and/or aggregations. In an attempt to overcome the latter issues (e.g. polydispersion) fractionation of the NCs was performed, being based on different centrifugal times (whilst keeping the centrifugal force constant) of water-diluted dispersions. The obtained fractions demonstrated extremely random-sized profiles for NC centrifugates, being irrespective of

Fig. 5 The DLS analysis of **a** average-size of native CNFs and CNCs, and their intensity size-distribution profile being recorded (before and after the labelling with 4 % RB4 dye) at pH 9.3 adjusted with **b** 0.1 M NaOH or **c** 20 mM borate buffer, without or with addition of 50 mM SDS. For better visualization of size distribution, graphs with normal size (nm) scale are inserted



measuring media (data not shown) as the consequence of very small differences in their masses/densities as major separation triggered during the centrifugal process.

Further examinations of the NCs in relation to their polydispersion and aggregation phenomenon were simplified by following 4 % RB4-labelled CNFs and CNCs, respectively, at pH 9.3 being adjusted with 0.1 M NaOH or by using 20 mM borate buffer, with and without of SDS addition.

It is worth mentioning that non-spherical particles' diffusions and consequently DLS-measured average-sizes are directly affected by changes in their lengths rather than diameters, therefore, the labelling process itself was not expected to greatly influence the NC average-sizes. However, the size-distribution intensity data (Fig. 5b) demonstrated the average sizes' increments after 4 % RB4 labelling from 340 ± 125 to 1106 ± 117 nm for CNFs and from 295 ± 26.2 to 458 ± 98 nm for CNCs, both being suspended in

water solution of pH 9.3 adjusted with 0.1 M NaOH. Such increments were obviously not direct consequences of dye attachments but rather the labelling-induced aggregation (which will be confirmed later by TEM and CPS analyses), being more significant for CNFs although, however, the peaks' shapes' narrowing (above all in the cases of labelled CNCs) also indicated more homogeneously-aggregated suspension on the NCs. A significant shift in the average size-distribution values towards even higher sizes for CNFs and peaks broadening for CNCs could be observed within a borate buffer solution (adjusted to the same pH, pH 9.3) (Fig. 5c), being a consequence of its surface's negative charge shielded by the buffer ions (as already presented by ζ -potential reduction) leading to further aggregation and polydispersity increments. The presence of a micellar concentration of SDS additionally alters the CNFs' size-intensity profiles towards higher values or peaks broadening for CNCs (in the cases of both solvents and using native NC), indicated by the formations of even larger aggregates or eventual overlapping by size-similar fractions. In contrast, insignificant changes of peaks' intensities but rather the peaks shifting back to lower values and their narrowing profiles in case of labelled NC, independent on the used medium for pH adjustment, may be claimed by the SDS attachment, as the average S-C₁₂ distance between the SDS molecules being between ~ 1.36 and ~ 1.46 nm (and depending on the salt concentrations) may form up to a 3 nm thin layer (Sammalkorpi et al. 2009), thus forming more equally distributed SDS-covered aggregates (Filipe et al. 2010).

A few additional small peaks within all of the DLS spectra could be observed. The peak at 68 ± 31 nm, identified only in native CNCs may arise from the PEG traces (being used for CNCs concentrations during their production) rather than from the labelled samples and as well as the formed PEG-SDS composite micelles, the sizes of which correspond to those already described in the literature (Guo et al. 2005). The presence of a small peak at around 2–6 nm, being related to the SDS-based micelles, formed during the applied concentration (Pérez-Rodríguez et al. 1998). In the cases of CNFs, the peak at 105 ± 22 nm may demonstrate the presence of trace fractions of hemicellulose/xylan (as already identified by FTIR), being desorbed from CNFs' in case of SDS presence or their complexity.

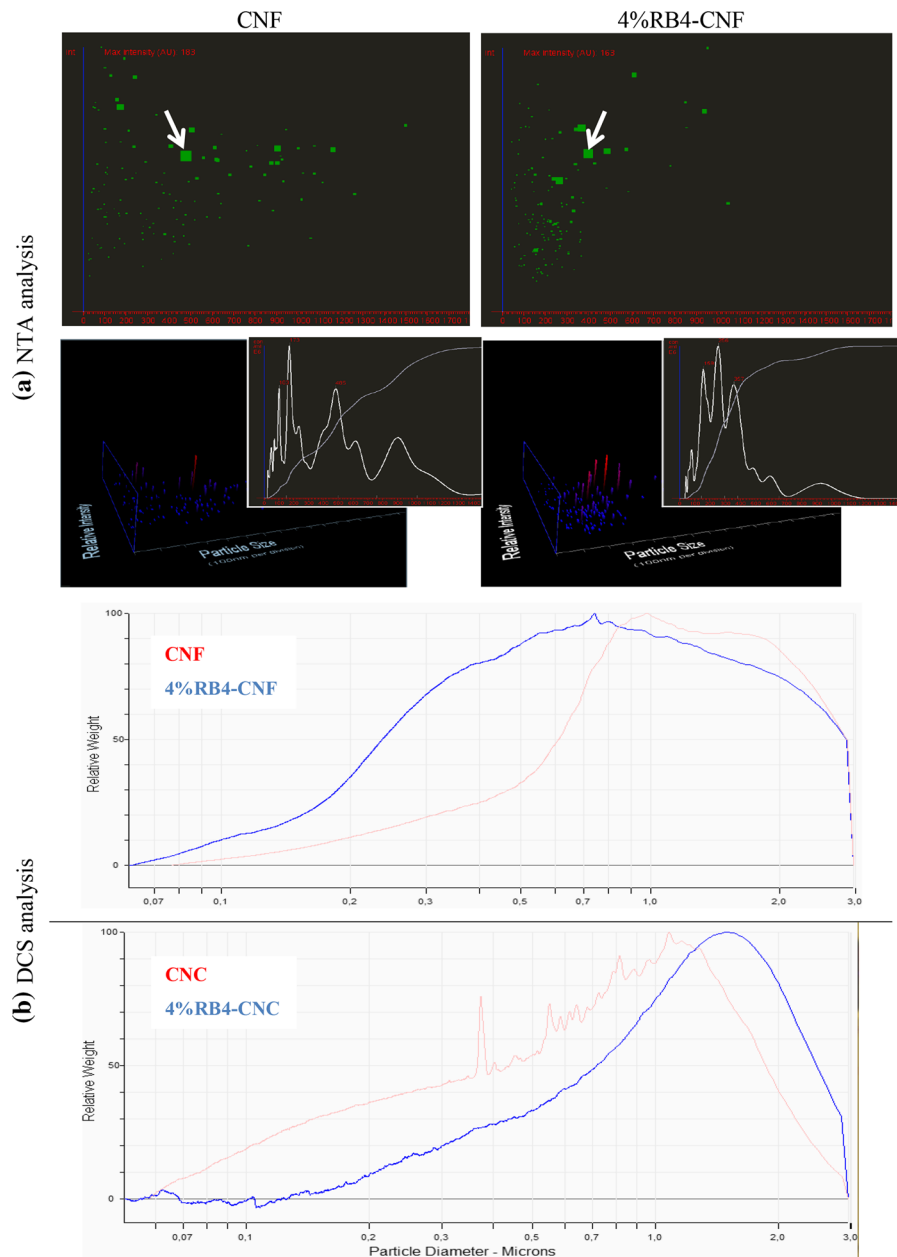
Characterisations of native and labelled-NC by NTA, DCS and TEM

The DLS technique is known to be extremely limited at its ability to resolve the very broad size distributions (high polydispersity) of particle sizes (as is ours), due to inherent ill-conditioned fit limitations associated with the de-convolutions of such complex exponentials. Moreover, the exponential correlation obtained by DLS is an intensity weighted measure which can be seriously influenced by larger particles, which contribute disproportionately to the signal detected by the used photon counting sensors.

Oppositely, the NTA measurement tracks the individual particle's Brownian motion trajectory, rather than averaging the bulk materials, making it sensitive for particles within the range of 10–2000 nm, being thus used as a more advance alternative analytical tool. The 2D scatter graphs, as presented in Fig. 6a, imply a reduction of the modest fraction (white arrows) after 4 % RB4 labelling of CNFs from ~ 500 to ~ 400 nm, which opposes the DLS findings due to the aforementioned reasons. This technique additionally revealed the presence of a significant quantity of additional fractions in the case of native-CNFs, being from a few nm up to 1500 nm in size, thus giving an apparent picture of their polydispersity. Anyhow, the detected overlapping peaks resulting from the inherent limitation of measuring stochastic process by sampling over a finite time period (Dragovic et al. 2011) needs additional software corrections, being beyond the scope of this paper. Moreover, the NTA was hardly applicable for CNCs analysis due to very intensive light scattering at the measuring concentrations.

On the other hand, the DCS analysis (Fig. 6b) detected a broadened size-distribution profile of the samples by its shifting towards smaller sizes within CNFs and towards size increases within CNCs after their labelling with 4 % RB4 dye. The broadening of size-distribution profile lines are well aligned with those from DLS analysis, although the absolute (measured) values were dissimilar (nor with NTA in the case of CNFs), due to the sedimentation phenomena being typical for non-spherical nanoparticles evaluated by these technique (Sharma et al. 2009). Moreover, the obtained phenomena of size shifting effect can be clearly explained from the TEM micrographs (Fig. 7), clearly identifying the labelling-induced conformation of cellulose nanofibrils

Fig. 6 The **a** NTA and **b** CPS analysis of CNFs and CNCs before and after the labelling with 4 % RB4



(CNFs), same as with the sequential aggregation of needle-like CNCs, obviously differing from their native (non-labelled) counterparts.

Characterisations of native and labelled-NC by CE and MKCE analyses

The capillary electrophoretic separation of nanoparticles has already been demonstrated as a useful tool for

identifying their surface modification changes and thus intrinsic versus electrophoretic properties (Oszwałdowski et al. 2011), even providing non-linear separation as for molecular and ionic solutes. According to the electrophoretic mobility equation ($\mu_p = q / 6\pi\eta r$ where η is viscosity coefficient of mobile phase, q is the charge, and r the hydrodynamic radius of analyte; Hwang et al. 2003), the μ_p is directly dependent on both ζ -potential and size as equivalents

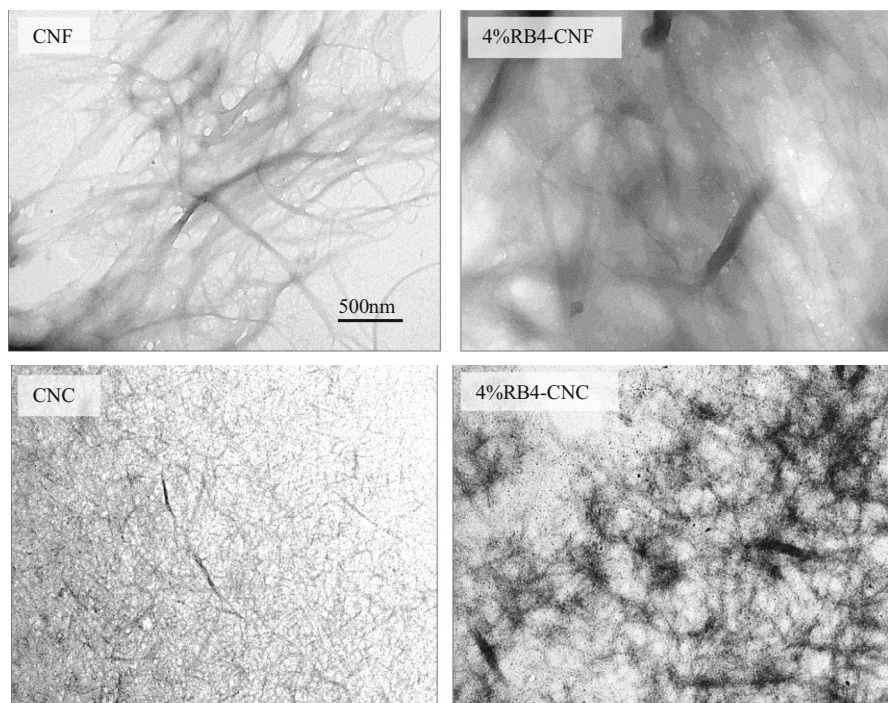


Fig. 7 The TEM images of CNFs and CNCs before (*left*) and after (*right*) the labelling with 4 % RB4

of q and r , respectively. This means that electrophoretic separation of both non-labelled and labelled NCs within the capillary, resulting from the electrophoretic mobility and electro-osmotic flow (EOF) as a counterpart force, would be guided by two variables, the charge and the size, and may be correlated when using the identical mobile phase (i.e. $\eta = \text{constant}$).

As both parameters varied in a rather complex fashion for native NCs (data not shown), the resulting electropherograms demonstrated relatively pure separation power, irrespective of the negative ζ -potential of NC (-10 mV for CNFs to -30 mV for CNCs, Fig. 4b) as well as the mobile (BGE) phase used (i.e. CE or MKCE modes). Therefore, neither CE nor MKCE were usable for precise separation of such highly aggregated and heterogeneous samples, showing the presence of several broad and unresolved peaks with unpredictable migration profiles (shape and time) at each run (not presented). Indeed, the aggregations in both samples obviously existed before being introduced into the capillary tube (as shown by the TEM image) but even overcome at that stage, it may have been brought about or speeded up by an external electric field (Radko and Chrambach 2002), as obviously appeared under CE

conditions. Moreover, since even the analyses of separate fractions (data not shown), same as DLS analysis, did not provide significant improvement in the peaks' sharpening, an asymmetrical peak being detected at 200 nm (being related to the cellulose-related carbonyl group adsorption).

Meanwhile the hydrophobic RB4 dye could not be analysed either under the CE conditions, probably due the same reasons (intensive aggregation in high pH media (ALDEGS et al. 2008) and consequent sedimentary effect. Oppositely, only one also very small resolved peak at about 1.7 min was identified at 598 nm within the MKCE electropherogram (in the presence of anionic surfactant SDS) (Fig. 8), which may be related to one of the possible (mono- or di-hydrolysed, or reactive) forms (Epolito et al. 2005), whilst the other two additional unresolved peaks appearing a few minutes later could be assigned to SDS micelles (b) and EOF marker tiourea (c), both being detectable only at 200 nm.

Interestingly, a relatively large peak within 4 % RB4-CNF of the CE electropherogram, having a migration time of about 6.43 min, was only identified at 200 nm and not at 598 nm, that may indicate a non-labelled CNF fraction with a broad size distribution

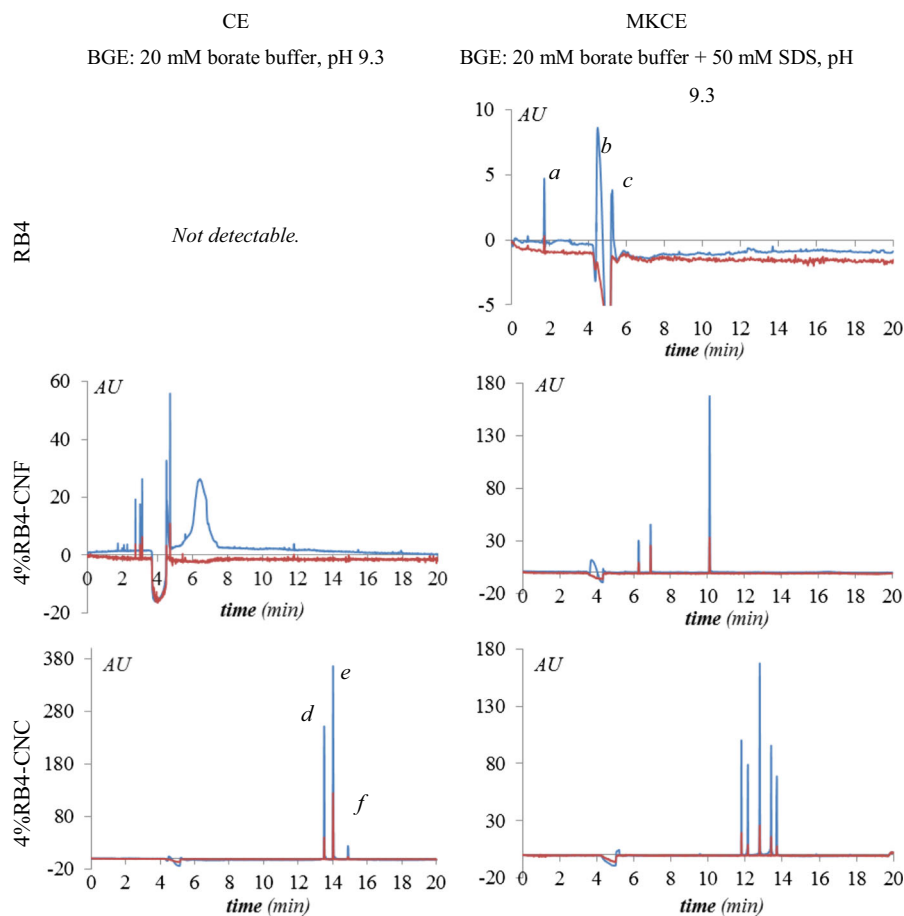


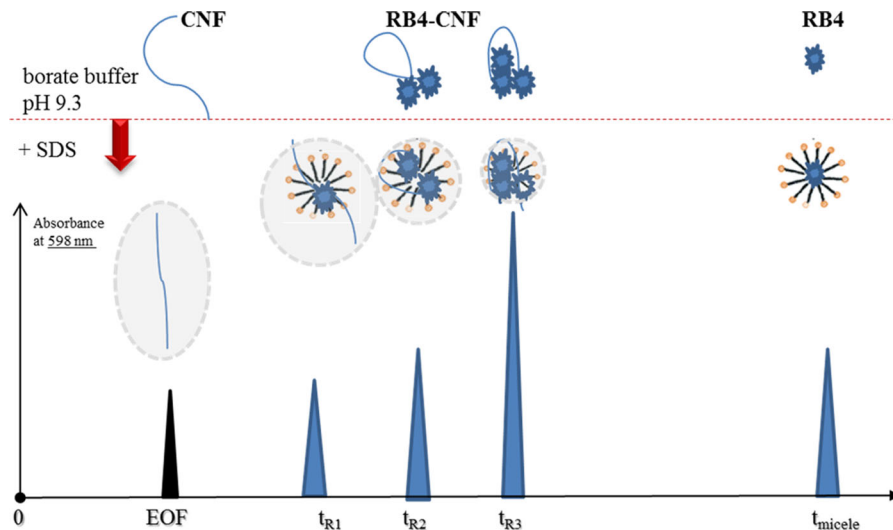
Fig. 8 CE/MKCE electropherograms of pure RB4 dye, as well as 4 % RB4-labelled CNFs and CNCs, obtained by DAD detection at 200 nm (blue) and 598 nm (red). (Color figure online)

profile, whilst several spike-like peaks within the 2–4.5 min region being identified at 598 nm, may be related to either the labelled CNFs or non-bonded and/or hydrolysed RB4 (Ojstrsek et al. 2008). Indeed, it has already been demonstrated that hydrolysed forms of RB4 are capable of being adsorbed rather than reacting with cellulose OH groups, behaving as direct/substantive dye and as such being hardly removable under washing procedures (Fernandez Cid et al. 2004). This demonstrates the capacity of CE to force desorption of non-bonded dye, thus separating labelled from non-labelled fractions, however, without meaningful further separation amongst each.

The introduction of SDS to the mobile phase (MKCE analysis) was expected to significantly improve the separation process as the SDS shell underestimated the charge difference between native

and labelled-CNFs, therefore the RB4-labelled CNFs migration times would become a size function, and because of the great affinity of SDS towards hydrophobic dye molecule segments (Hancu et al. 2013) lowering the dye- (and dye-labelled NC) migration velocity. As seen from Fig. 8, the 4 % RB4-labelled CNFs showed a spike-like right shoulder at t_r of 4 min immediately after the EOF-related negative peak, being assigned to the tiourea marker (the t_r is shifted compared to pure RB4 solution due different viscosities) and followed by three more peaks (t_r at 6.27, 6.91 and 10.11 min) all of them being detectable at both inspected wavelengths. According to the separation principle we may speculate that only the first peak is related to the RB4 dye molecules, the second to hydrodynamically larger CNFs' having lower quantities of bonded RB4 dye molecules, and the third (with

Scheme 2 Tentative mechanism of separation dynamic of hydrophobic RB4 dye and quantitatively-differently labelled CNFs



the largest signal intensity) to the CNFs with higher RB4 concentrations, according to the tentative mechanism presented in Scheme 2. This mechanism can be supported by the fact that both CNF' amorphous regions, same as the dye-related hydrophobic moiety within RB4-labelled CNFs, may undergo dye-concentration dependent conformation changes within water-based media. This would lower their hydrodynamic sizes, as also demonstrated by NTA and TEM images, which however is hardly a measuring phenomenon due to that already proved (by DLS and CPS) extensive aggregation. A same profile with less than half the peak intensity was detected for 2 % RB4 (data not presented).

In contrast, the CE of 4 % RB4-CNC identified three well-resolved peaks within the 13–15 min region, amongst which the first two very intensive ones may be attributed to RB4-labelled CNCs, whilst the narrowest and last peak could present desorbed (non)hydrolysed dye. In addition, the additional peaks detected at both wavelengths within the EOF-related (–) region (between 4 and 6 min), indicate the presence of labelled fractions without sufficient separation power being related to low RB4 content. The BGE modification with SDS addition (MKCE), further improved the separation of these two main fractions, being seen with two additional peaks. However, speculated dye-concentration-dependent conformational changes, visible by the increasing peaks' intensities within the MKCE electropherogram of RB4-

labelled CNFs were unobserved here, being explainable due to the rigidity of the highly crystalline system.

Conclusion

The setting-up of complementary analytical tools with different time-scale tracing capacities as well as resolution and sensitivity profiles (i.e. DLS, CPS, NTA, TEM, and CE/MKCE) was used to follow and assess the polydispersity and assembling of native and by hydrophobic dye covalently-labelled cellulose nanofibrils and cellulose nanocrystals. Whilst DLS brings semi-quantitative information of labelling-induced nanofibrils aggregation, the DCS and NTA analysis, being combined with TEM visualisation, qualitatively supports their association phenomena, same as the polydispersity. In addition, the feasibility of CE for electrophoretically-induced desorption of highly substantive and chemically non-bonded dye from nanocellulose demonstrate its applicability as a preparative tool, being further extended by evaluation of nanofibrils' conformational changes by using MKCE.

Acknowledgments This research was financially supported by the European Commission under the NanoSelect project (Contract No. FP7-NMP4-SL-2012-280519), Slovenian Ministry of Education, Science, Culture and Sport under the MNT Era-Net programme (Project No. POSSCOG), and QualityNano project (Grant No. INFRA-2010-262163).

References

- Abitbol T et al (2013) Fluorescent labeling and characterization of cellulose nanocrystals with varying charge contents. *Biomacromolecules* 14(9):3278–3284
- Bendahou A et al (2014) Esterification and amidation for grafting long aliphatic chains on to cellulose nanocrystals: a comparative study. *Res Chem Intermed* 41:1–18
- Aldegs Y et al (2008) Effect of solution pH, ionic strength, and temperature on adsorption behavior of reactive dyes on activated carbon. *Dyes Pigm* 77(1):16–23
- Choi HS, Frangioni JV (2010) Nanoparticles for biomedical imaging: fundamentals of clinical translation. *Mol Imaging* 9(6):291–310
- Christiane A, Steeve M, Jean-Bosco ST, Kor NM, Brama I, Eric G, Philippe G (2013) Biodegradation of reactive blue 4 and orange G by *Pycnoporus sanguineus* strain isolated in Gabon. *J Bioremediat Biodegrad* 4:1–7
- Domingues RMA, Gomes ME, Reis RL (2014) The potential of cellulose nanocrystals in tissue engineering strategies. *Biomacromolecules* 15(7):2327–2346
- Dong S, Roman M (2007) Fluorescently labeled cellulose nanocrystals for bioimaging applications. *J Am Chem Soc* 129(45):13810–13811
- Dragovic RA et al (2011) Sizing and phenotyping of cellular vesicles using nanoparticle tracking analysis. *Nanomed Nanotechnol Biol Med* 7(6):780–788
- Dufresne A (2012) Nanocellulose: from nature to high performance tailored materials. Walter de Gruyter, Boston
- Dufresne A (2013) Nanocellulose: a new ageless bionanomaterial. *Mater Today* 16(6):220–227
- Epolito W et al (2005) Characterization of the textile anthraquinone dye Reactive Blue 4. *Dyes Pigm* 67(1):35–46
- Eyley S, Thielemans W (2014) Surface modification of cellulose nanocrystals. *Nanoscale* 6(14):7764–7779
- Fall A (2013) Colloidal interactions and orientation of nanocellulose particles. Doctoral thesis, KTH Royal Institute of Technology, Stockholm, 49 p
- Fernandez Cid MV et al (2004) Kinetics study of a dichlorotriazine reactive dye in supercritical carbon dioxide. *J Supercrit Fluids* 32(1–3):147–152
- Filipe V, Hawe A, Jiskoot W (2010) Critical evaluation of nanoparticle tracking analysis (NTA) by NanoSight for the measurement of nanoparticles and protein aggregates. *Pharm Res* 27(5):796–810
- Generalova AN et al (2009) Highly fluorescent ethyl cellulose nanoparticles containing embedded semiconductor nanocrystals. *Colloids Surf A* 342(1–3):59–64
- Granja PL et al (2001) Cellulose phosphates as biomaterials. I. Synthesis and characterization of highly phosphorylated cellulose gels. *J Appl Polym Sci* 82(13):3341–3353
- Guo W et al (2005) Interaction of PEG with ionic surfactant SDS to form template for mesoporous material. *Colloids Surf A* 252(1):71–77
- Habibi Y, Lucia LA, Rojas OJ (2010) Cellulose nanocrystals: chemistry, self-assembly, and applications. *Chem Rev* 110(6):3479–3500
- Halonen H, Larsson PT, Iversen T (2012) Mercerized cellulose biocomposites: a study of influence of mercerization on cellulose supramolecular structure, water retention value and tensile properties. *Cellulose* 20(1):57–65
- Hancu G et al (2013) Principles of micellar electrokinetic capillary chromatography applied in pharmaceutical analysis. *Adv Pharma Bull* 3(1):1–8
- Huang J-L, Li C-J, Gray DG (2013) Cellulose nanocrystals incorporating fluorescent methylcoumarin groups. *ACS Sustain Chem Eng* 1(9):1160–1164
- Hwang W et al (2003) Separation of nanoparticles in different sizes and compositions by capillary electrophoresis. *Bull Korean Chem Soc* 24(5):684–686
- Ioelovich M (2009) Nano-structural concept of papermaking. *J Sita* 11(1):52–60
- Islam MT, Alam MM, Zoccola M (2013) Review on modification of nanocellulose for application in composites. *Int J Innov Res Sci Eng Technol* 2(10):5444–5451
- Iwamoto S, Lee S-H, Endo T (2013) Relationship between aspect ratio and suspension viscosity of wood cellulose nanofibers. *Polym J* 46(1):73–76
- Jiang F, Hsieh Y-L (2013) Chemically and mechanically isolated nanocellulose and their self-assembled structures. *Carbohydr Polym* 95(1):32–40
- Jonoobi M, Mathew AP, Oksman K (2012) Producing low-cost cellulose nanofiber from sludge as new source of raw materials. *Ind Crops Prod* 40:232–238
- Jorfi M, Foster EJ (2014) Recent advances in nanocellulose for biomedical applications. *J Appl Polym Sci* 132(14). doi:10.1002/APP.41719
- Kim J et al (2009) Dispersion of cellulose crystallites by non-ionic surfactants in a hydrophobic polymer matrix. *Polym Eng Sci* 49(10):2054–2061
- Lin N, Dufresne A (2014) Nanocellulose in biomedicine: current status and future prospect. *Eur Polymer J* 59:302–325
- Lindström T, Aulin C (2014) Market and technical challenges and opportunities in the area of innovative new materials and composites based on nanocellulosics. *Scand J For Res* 29(4):345–351
- Liu P et al (2013) Cellulose and chitin nanomaterials for capturing silver ions (Ag⁺) from water via surface adsorption. *Cellulose* 21(1):449–461
- Mariño M et al (2015) Enhanced materials from nature: nanocellulose from citrus waste. *Molecules* 20(4):5908–5923
- Missoum K, Belgacem M, Bras J (2013) Nanofibrillated cellulose surface modification: a review. *Materials* 6(5):1745–1766
- Ojstrsek A, Doliska A, Fakin D (2008) Analysis of reactive dyestuffs and their hydrolysis by capillary electrophoresis. *Anal Sci* 24(12):1581–1587
- Oksman K et al (2011) Cellulose nanowhiskers separated from a bio-residue from wood bioethanol production. *Biomass Bioenergy* 35(1):146–152
- Oszwałdowski S, Zawistowska-Gibuła K, Roberts KP (2011) Capillary electrophoretic separation of nanoparticles. *Anal Bioanal Chem* 399(8):2831–2842
- Park S et al (2009) Measuring the crystallinity index of cellulose by solid state ¹³C nuclear magnetic resonance. *Cellulose* 16(4):641–647
- Pérez-Rodríguez M et al (1998) A comparative study of the determination of the critical micelle concentration by conductivity and dielectric constant measurements. *Langmuir* 14(16):4422–4426

- Radko SP, Chrambach A (2002) Separation and characterization of sub-microm- and microm-sized particles by capillary zone electrophoresis. *Electrophoresis* 23(13):1957–1972
- Roman M (2015) Toxicity of cellulose nanocrystals: a review. *Ind Biotechnol* 11:25–33
- Rosa MF et al (2010) Cellulose nanowhiskers from coconut husk fibers: effect of preparation conditions on their thermal and morphological behavior. *Carbohydr Polym* 81(1):83–92
- Sammalkorpi M, Karttunen M, Haataja M (2009) Ionic surfactant aggregates in saline solutions: sodium dodecyl sulfate (SDS) in the presence of excess sodium chloride (NaCl) or calcium chloride (CaCl₂). *J Phys Chem B* 113(17):5863–5870
- Sharma V, Park K, Srinivasarao M (2009) Shape separation of gold nanorods using centrifugation. *Proc Natl Acad Sci USA* 106(13):4981–4985
- Shi L, Fu Y (2011) Isolation, purification, and immunomodulatory activity in vitro of three polysaccharides from roots of *Cudrania tricuspidata*. *Acta Biochim Biophys Sin* 43(5):418–424
- Srikulkit K, Pomsuriyasak P (1998) Method of chemical modification of cellulosic fibers to improve their dyeability with reactive dyes. *J Sci Res Chula Univ* 23:143–153
- Sun R-C (2009) Detoxification and separation of lignocellulosic biomass prior to fermentation for bioethanol production by removal of lignin and hemicelluloses. *Bioresources* 4(2):452–455
- Sun D et al (2013) Adsorption of reactive dyes on activated carbon developed from *Enteromorpha prolifera*. *Am J Anal Chem* 04(07):17–26
- Xu X et al (2013) Cellulose nanocrystals vs. cellulose nanofibrils: a comparative study on their microstructures and effects as polymer reinforcing agents. *ACS Appl Mater Interfaces* 5(8):2999–3009
- Zoppe JO (2011) Surface modification of nanocellulose substrates. Dissertation, North Carolina State University, Ann Arbor